Journal of Magnetic Resonance 210 (2011) 159–170

Contents lists available at ScienceDirect

Journal of Magnetic Resonance

journal homepage: www.elsevier.com/locate/jmr

Perspectives in Magnetic Resonance

Solution NMR spectroscopy of supra-molecular systems, why bother? A methyl-TROSY view

Lewis E. Kay *

Departments of Molecular Genetics, Biochemistry and Chemistry, The University of Toronto, Toronto, Ontario, Canada M5S 1A8

ARTICLE INFO

Article history:
Received 14 January 2011
Revised 3 March 2011
Available online 8 March 2011

Keywords:
Methyl-TROSY
HMQC
Proteasome
Methyl labeling
Protein dynamics
Supra-molecular systems

ABSTRACT

With the development of appropriate labeling schemes and the associated experiments that exploit them it has become possible to record high quality solution NMR spectra of supra-molecular complexes with molecular masses extending to 1 MDa. One such approach involves selective $^{13}CH_3$ methyl labeling in highly deuterated proteins using experiments that make use of a methyl-TROSY effect that significantly improves both resolution and sensitivity in spectra. The utility of this methodology has been demonstrated on a growing number of interesting particles. It seems appropriate at this juncture, therefore, to 'step back' and evaluate the role that solution NMR spectroscopy can play in what has traditionally been the domain of X-ray crystallography and more recently cryo-electron microscopy. It is argued here that solution NMR can make a critical contribution to our understanding of how dynamics regulate function in these high molecular weight systems. Several examples from work in my laboratory on the proteasome are presented as an illustration.

1. Introduction

Many critically important processes in the cell are regulated by very large molecular complexes acting essentially as microscopic machines [1]. Like their macroscopic counterparts, these tiny machines are not static. They contain movable 'parts' and the changes in conformation that occur are very often crucial for proper function [2]. Not surprisingly, an understanding of the way that these systems work has been a longstanding goal of biochemists and structural biologists alike. Some of the more famous molecules whose detailed crystallographic study has lead to Nobel Prizes include the photosynthetic reaction center (J. Deisenhofer, R. Huber, H. Michel, 1988) [3,4], F_1 ATPase (J. Walker, 1997) [5], RNA polymerase (R. Kornberg, 2006) [6,7] and the 30S and 50S ribosome subunits (A. Yonath, T. Steitz, V. Ramakrishnan, 2009) [8–10]. Structures of other important large complexes, such as the chaperone GroEL/GroES [11], the proteasome [12], the exosome [13] and virus particles [14] have also emerged from X-ray studies and all have played an important role in developing our understanding of vital biochemical events at the molecular level.

Of course X-ray crystallography is not the only method for obtaining high resolution structures of biomolecules. In the past several decades solution-state NMR spectroscopy [16–18], and more recently solid state NMR spectroscopy [15,16], have emerged as *bona fide* methods for solving atomic resolution structures. Yet, despite all the important technical advances, encompassing new experiments, novel expression systems, higher magnetic fields and increased sensitivity, there still remains a significant size barrier to NMR studies. For example, molecules or complexes larger than 50–100 kDa (and in some cases even much smaller) often pose a significant challenge to traditional backbone-directed triple resonance multi-dimensional solution NMR experiments that have proven so useful for smaller systems [17,18]. It is certainly the case that similar solution triple resonance studies of complexes with aggregate molecular masses in the hundreds or perhaps thousands of kDa will, for the most part, not be possible. This raises an interesting question. Given that the 'traditional NMR approach' entailing assignment of all ^1H, ^{13}C and ^{15}N spins in the molecule, followed by detailed structural analyses, is very likely to fail in studies of supra-molecular systems, is there a role that solution NMR can nevertheless play in providing important structural insights into the function of such large molecules? And what might such a role be? These questions become even more relevant against the backdrop of beautiful and detailed (static) pictures that have been produced by X-ray techniques that in many cases have revolutionized our thinking about biomolecular function.

In this perspective I will briefly review an approach that my laboratory has developed over the past 15 years for studies of very high molecular weight protein complexes by solution NMR and illustrate, with examples from our research on the proteasome, how this methodology can make valuable contributions to the understanding of structure, dynamics and function in very large systems. The goal here is not to be comprehensive, nor is it to

* Fax: +1 416 978 6885.
E-mail addresses: kay@pound.med.utoronto.ca, kay@bloch.med.utoronto.ca

1090-7807/$ - see front matter © 2011 Elsevier Inc. All rights reserved.
doi:10.1016/j.jmr.2011.03.008

review the literature. The interested reader is referred to other articles [19–23] to find additional examples of how solution NMR can be used to provide important molecular insights in ways that even the most detailed X-ray structures cannot.

2. A simple strategy for preserving magnetization emerges from a complex spin system

One promising approach for studies of very high molecular weight proteins involves producing [^{12}C,^{2}H]-labeled molecules where ^{13}C and ^{1}H spins are incorporated into methyl positions [24]. Initial strategies focused on methyls of Ile (δ1), as well as Leu/Val, where in the latter case only one of the two prochiral methyl groups is $^{13}CH_3$ (the other is $^{12}CD_3$), using commercially available precursors [25]. More recently, biosynthetic strategies for producing proteins with $^{13}CH_3$ labeling at Ala [26,27], Met [28], Ile ($C^{\gamma 2}$) [29] as well as stereospecific incorporation of methyl label into Leu, Val *proR* or *proS* positions [30] have emerged. The reason why methyl groups are so useful as probes in supra-molecules can be understood by considering the energy level diagram for an isolated $^{13}CH_3$ spin system, Fig. 1A. The large number of transitions may seem daunting at first, but in fact this complexity can be used efficiently to construct magnetization transfer pathways where relaxation losses in experiments are minimized [31]. Assuming that the methyl group rotates rapidly about its threefold axis, which in turn is attached to a molecule that tumbles slowly in solution (macromolecular limit) it can be shown that coherences either relax very slowly or very rapidly and that the relaxation of each transition is effectively single exponential [31,32]. In Fig. 1A rapidly and slowly relaxing ^{1}H single-quantum transitions are denoted by vertical arrows (red = rapid, blue = slow), ^{13}C single-quantum transitions are denoted by the black and gray arrows corresponding to rapid or slow decay, respectively, and ^{1}H–^{13}C double-/zero-quantum transitions are depicted with purple (fast) and green (slow) colored arrows. Pulse schemes that give rise to spectra with high sensitivity are those that navigate the 'energy landscape' in such a way so that magnetization is always transferred between slowly relaxing transitions. Fig. 1B highlights the simplest of experiments, the ^{1}H–^{13}C standard HMQC scheme [33,34], that exploits a methyl-TROSY effect to produce high quality data sets. Magnetization originating from the slowly relaxing ^{1}H transitions (blue) is transferred to slowly relaxing ^{1}H–^{13}C double-/zero-quantum coherences (green) and then back to the slowly relaxing ^{1}H magnetization for detection. In contrast, the second of the two possible transfer pathways involves exclusively rapidly relaxing components that contributes very little to spectra of high molecular weight proteins. Central to the efficacy of this approach is the use of highly deuterated, methyl protonated proteins so as to minimize ^{1}H–^{1}H cross-relaxation and hence increase the 'isolation' between the fast and slowly relaxing pathways, similar to the role of deuteration in the case of ^{1}H–^{15}N TROSY [35].

The utility of the methyl-TROSY approach has been demonstrated with many applications involving a large number of systems [19–23,36–40]. In Fig. 2 three proteins are highlighted that

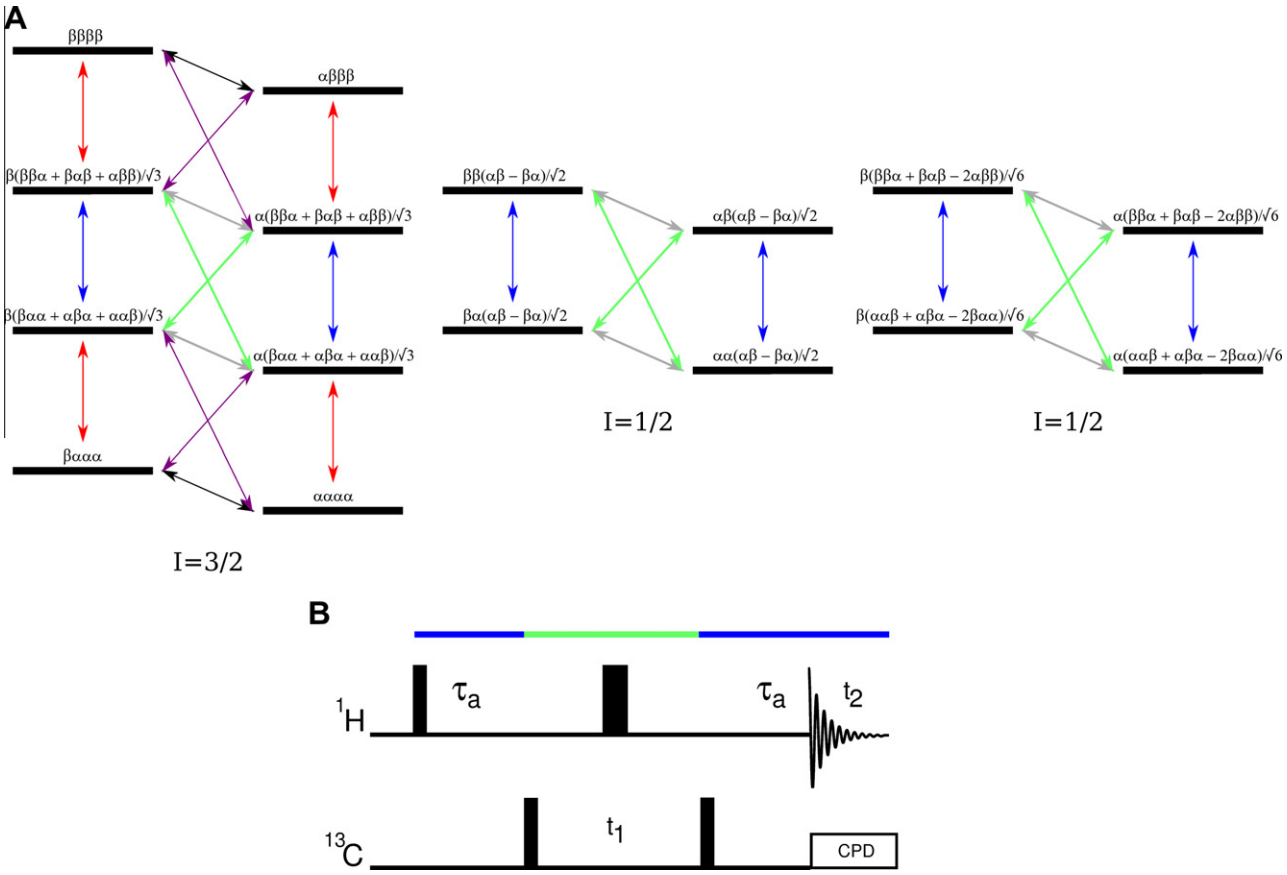

Fig. 1. (A) Energy level diagram for an isolated $^{13}CH_3$ spin system with wave functions written in an irreducible basis representation. The first spin state in each function corresponds to the ^{13}C spin, with the remaining associated with the ^{1}H spins. The total spin angular momentum of each manifold is listed along with the ^{1}H transitions (vertical lines; red and blue corresponding to fast and slow relaxing transitions), ^{13}C transitions (horizontal lines; black and gray indicate fast and slowly relaxing transitions) and ^{1}H–^{13}C double-/zero-quantum transitions (purple = fast, green = slow). Adapted from Tugarinov et al. [31]. (B) ^{1}H–^{13}C HMQC pulse scheme that exploits a methyl-TROSY effect to generate spectra of high sensitivity and resolution. Coherences operative during the sequence are highlighted in the same colors as in (A).

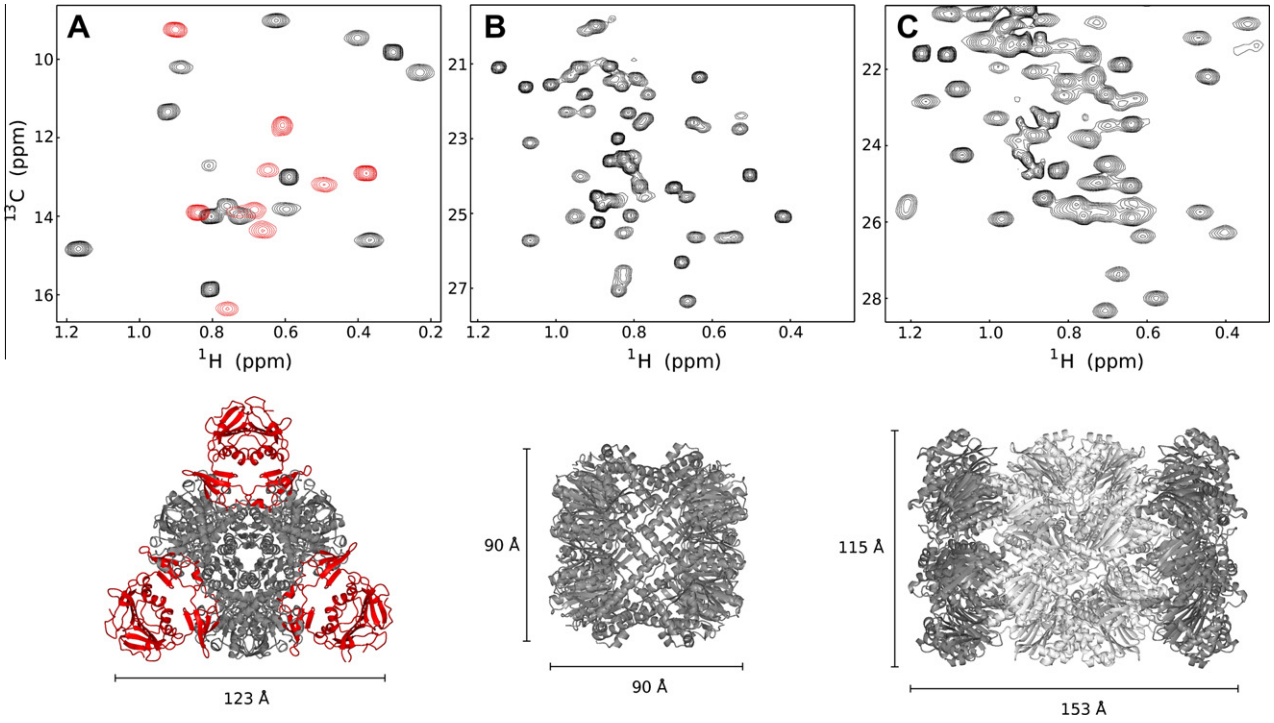

Fig. 2. Selected regions of ^{1}H–^{13}C HMQC spectra of U-[^{2}H] Ile-[$\delta1^{13}CH_3$]-aspartate transcarbamoylase (A: 300 kDa, 37 °C, red = R domain; black = C domain) [19], U-[^{2}H] Ile-[$\delta1^{13}CH_3$] Leu, Val-[$^{13}CH_3$,$^{12}CD_3$]-ClpP (B: 300 kDa, 50 °C) and U-[^{2}H] Ile-[$\delta1^{13}CH_3$] Leu, Val-[$^{13}CH_3$,$^{12}CD_3$]-proteasome (C: 670 kDa, 65 °C; only the α subunits are labeled) [38]. All data sets were recorded at a static magnetic field of 18.8 T using a spectrometer equipped with a room-temperature probe-head. Shown also are the X-ray derived structures of each protein complex [12,60,61] and the dimensions of each molecule. (For interpretation of the references to color in this figure legend, the reader is referred to the web version of this article.)

are among those studied in my laboratory, including aspartate transcarbamoylase (A: 300 kDa) [19], the ClpP protease (B: 300 kDa) and the proteasome (C: 670 kDa) [38]. High quality data sets are obtained in measurement times of 1–2 h in cases where monomer concentrations are on the order of a few hundred μM.

3. NMR Studies of the proteasome are complementary to high resolution crystallography

3.1. The dynamic proteasome gate

The 20S core particle (CP) proteasome is a hollow barrel-like structure that regulates processes such as protein degradation, cell division, signaling and gene expression [41,42] and is the focus of efforts towards the design of effective inhibitors of function [43]. The CP is composed of four homo-heptameric rings, and in the case of the *T. acidiphilum* (archaeal) version that is studied by my group each ring consists of seven identical monomers ($\alpha_7\beta_7\beta_7\alpha_7$), forming three chambers, including a pair of antechambers (formed by $\alpha_7\beta_7$) and a catalytic chamber (formed by $\beta_7\beta_7$) that sequesters the active sites [12], Fig. 3A. Unfolded substrates enter the 20S CP from the top and the bottom, through the α-annulus that in turn is occluded by the N-termini of the 7 α-subunits of each α_7 ring which gate access of substrate. An understanding of the mechanism by which these termini function as gates is therefore critical for a description of how the 20S CP is regulated. Yet the high resolution X-ray structure of the archaeal proteasome [12], which has established the architecture of the barrel and has provided insight into the catalytic mechanism of substrate degradation, provides little insight into the gating mechanism since the complete trace of the α-subunit amino-terminal residues is not observed in density maps.

In an effort to address how gating might work in the *T. acidiphilum* 20S CP, studies were undertaken on the full 20S CP (Fig. 3A), on an $\alpha_7\alpha_7$ 'half proteasome' that forms spontaneously from wild-type (WT) α-subunits (Fig. 3B) [38], on an α_7 'quarter proteasome' that is comprised of α-subunits mutated in positions that occupy the interface between two rings so that only a single ring structure is stable (Fig. 3C) [21], and on an α-subunit that is mutated so that it is stabilized as a monomer in solution (Fig. 3D) [38]. Initially our focus was on using α_7 for which high quality ^{1}H–^{15}N TROSY data sets were recorded previously [21]. Approximately 90% of the amide correlations that were observable in ^{1}H–^{15}N TROSY data sets of the 180 kDa α_7 ring could be assigned from a comparison with spectra that were recorded on the single α-particle in concert with 3D HNCA and ^{15}N-edited NOESY data sets obtained on the ring. Regrettably 30% of the expected cross-peaks were not observed in any spectrum. The regions of the α-subunit (in the context of the α_7 ring) where data were lacking are shown in red in Fig. 4A and include the N-terminus of the protein, extending through helix H0 [21]. This is precisely the area of interest since as discussed above the gates are formed by the N-terminal (approximately ten) residues of each α-subunit; thus it was clear that ^{1}H–^{15}N based spectroscopy would not be of use in addressing questions relating to gating. Next ^{1}H–^{13}C data sets were recorded of a set of molecules with each containing one mutation in which an Ile residue was substituted into the terminus of the α-subunit [39]. In this manner methyl probes are 'engineered' into the gates that can be used to quantify their structure and dynamics. Fig. 4B shows a number of spectra recorded on U-[^{2}H] Ile $\delta1$-[$^{13}CH_3$] labeled $\alpha_7\alpha_7$ of single mutant proteins (Met1Ile, Gly4Ile, Ala7Ile) with the positions of the peaks corresponding to the added Ile highlighted. Although each of the new correlations can be observed their intensities are low. By means of comparison, signal-to-noise is much higher for the other

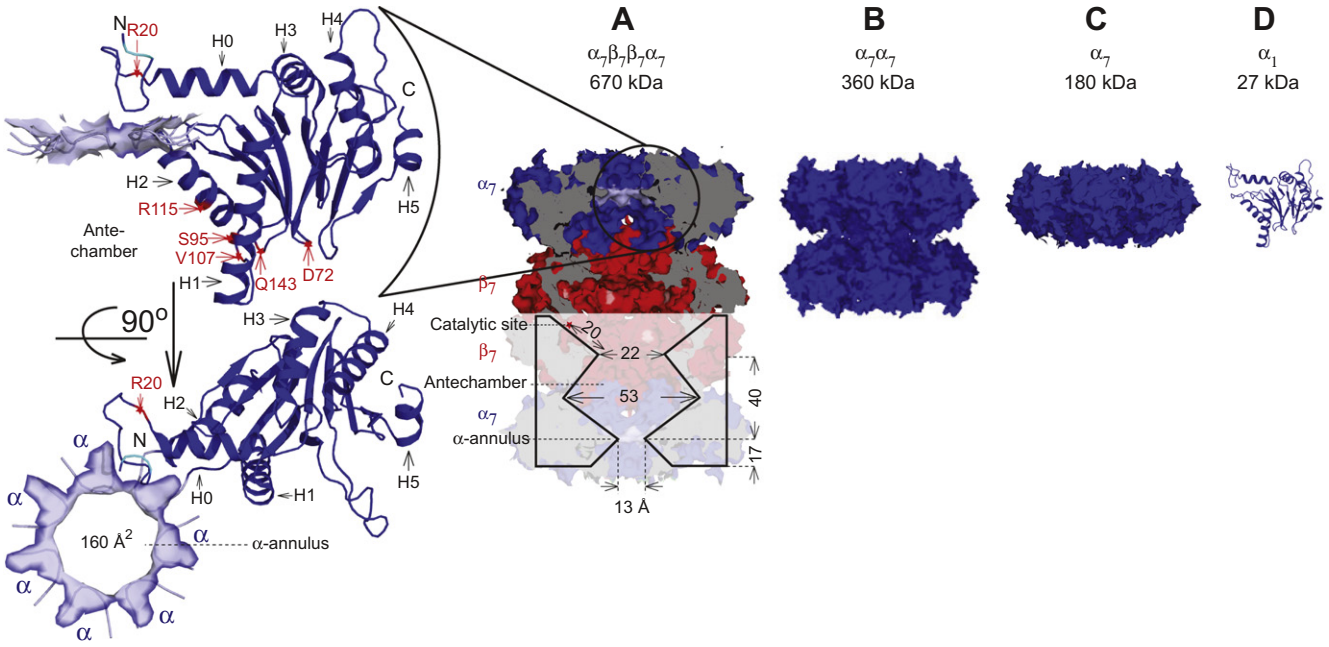

Fig. 3. Molecules used in proteasome studies [21,38–40], including the full 20S CP (A), an $\alpha_7\alpha_7$ '½ proteasome' (B), an α_7 '¼ proteasome' (C), and an α-subunit (D). Shown also in A is a single α-subunit (2 orientations), along with the α-annulus that is composed of residues from all seven subunits [12]. The locations of added spin-labels for PRE measurements are indicated in red. Adapted from Religa et al. [39].

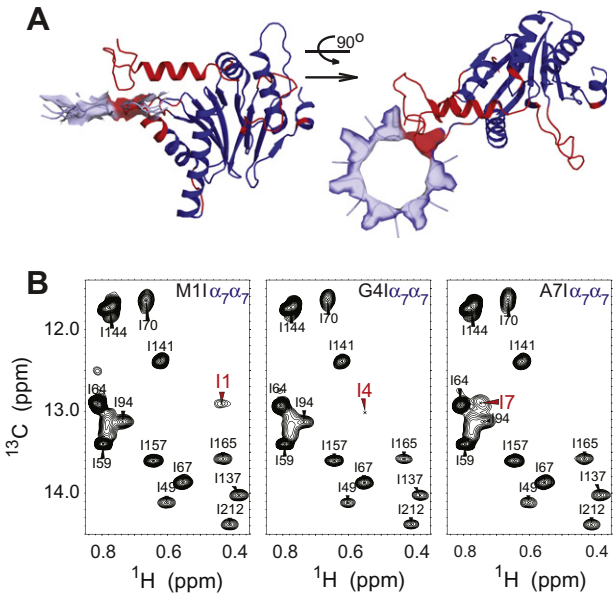

Fig. 4. (A) Ribbon diagram showing a single α-subunit [12] highlighting those regions of structure for which backbone amide correlation peaks were not observed in ^{1}H–^{15}N TROSY based spectra of α_7 (indicated in red) [21]. Also shown is the α-annulus that is composed of residues from all 7 α-subunits. A large portion of the 'invisible' residues are localized in and around the gating area, including from M1 to S35. (B) ^{1}H–^{13}C HMQC datasets recorded on U-^{2}H, Ile-[$^{13}CH_3\delta1$] $\alpha_7\alpha_7$, 50 °C, with Ile probes inserted into the gating termini of the α-subunits via mutagenesis. Although strong peaks are observed for the majority of Ile δ1 methyl groups, only very weak correlations are obtained for Ile1, 4 or 7 (red). Modified from Religa et al. [39].

Ile correlations that derive from residues that are removed from the gate. It is clear that the same dynamic process that is responsible for peak disappearance in ^{1}H–^{15}N spectra is contributing to the attenuation of Ile methyl peaks in the amino-terminal region of each α-subunit.

We next turned to a labeling scheme in which highly deuterated $^{13}CH_3$-Met proteins were produced, hoping that better quality spectra could be obtained [39]. The advantage of Met is twofold. First there are only five Met residues in the protein, with three of the five Met residues in the gate (M-1, M1 and M6). Thus, Met provides excellent 'coverage' of the N-terminal region of the α-subunit. Second, Met is the most dynamic of the methyl containing side-chains in proteins; methyl threefold axes order parameters squared tend to be between 0.1 and 0.2 for Met, significantly lower than for other methyl groups [44]. The hope was, therefore, that the rapid dynamics that are intrinsic to Met methyl groups would reduce the effects of the slower motional processes that lead to spectral attenuation.

Fig. 5 shows ^{1}H–^{13}C HMQC spectra recorded on highly deuterated $^{13}CH_3$-Met samples of α_7 (A), of WT $\alpha_7\beta_7\beta_7\alpha_7$ (B), of a double mutant of α_7 where Tyr and Asp at positions 8 and 9 are replaced by Gly (C), and of the monomeric version of the α subunit, α_1 (D). Notably, spectra of both the single ring and of the full proteasome contain more than the 5 peaks expected (Met-1, Met1, Met6, Met40, Met120). By contrast, data sets recorded on the monomer have the right number of peaks (the resonance for Met120 is outside the spectral window plotted). Clearly something about the ring structure is responsible for the appearance of the 'additional' correlations.

As a first step to understand the origin of the excess cross-peaks, Met correlations were assigned to specific sites in the protein through a mutagenesis strategy in which Met residues were replaced by Ala or Ile [39]. Interestingly, three correlations were derived for Met-1 and Met1, denoted by 'A' (major state), 'B' and 'C' (minor states) while a pair of correlations was noted for Met6 in the Y8G/D9G α_7 sample. The next step is to assign these multiple correlations to specific structural features of the proteasome, a much more difficult task than sequential assignment. Here paramagnetic relaxation enhancement (PRE) was used whereby nitroxide spin labels were attached to specific sites on the α-subunits of the α_7 ring [39]. Initially a nitroxide was affixed to position 4 (by

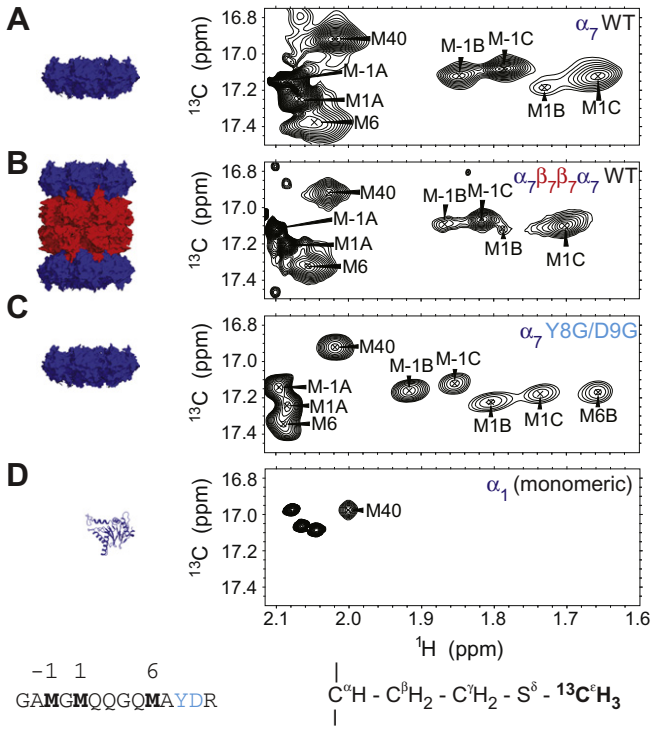

Fig. 5. ^{1}H–^{13}C HMQC datasets recorded on highly deuterated, $^{13}CH_3$-Met labeled WT α_7 (A), WT $\alpha_7\beta_7\beta_7\alpha_7$ (B), Y8G/D9G α_7 (C) and α_1 (D). Assignments of the Met residues are indicted on the spectra, where labels 'A', 'B', and 'C' denote different cross-peaks for a given Met residue [39]. Also shown is the primary sequence for the N-terminal 14 residues of the α-subunit that function in a gating role in the proteasome, as well as the structure of the amino acid Met. Modified from Religa et al. [39].

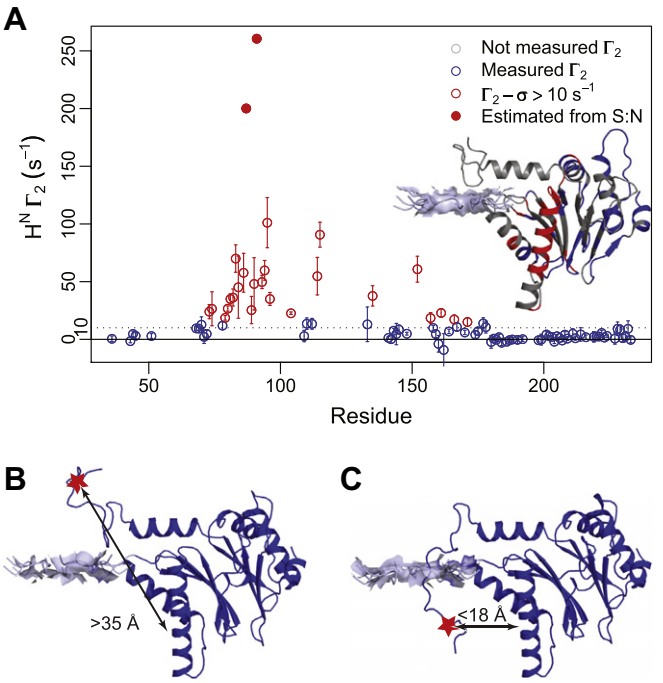

Fig. 6. (A) Amide proton Γ_2 (PRE) rates (the difference between ^{1}H transverse relaxation rates in the oxidized and reduced forms) quantified on a sample with a nitroxide (TEMPO) spin label attached to position 4 of each α-subunit of the WT α_7 particle [39]. Red open circles indicate those residues for which rates exceed measurement errors (σ) by at least 10 s^{-1}, while peaks for Val87 and Phe91 disappeared in the oxidized state (filled red circles). Rates were high for residues in helices H1 and H2, indicated in red in the inset. Note that amides of residues 1–35 are not visible in spectra due to a μs-ms exchange process and are thus not available as probes [21]. (B) Ribbon diagram of the α-subunit structure, placing the gating terminal residues above the α-annulus. The position of the spin label (red star) is indicated. Note that the distance from the label to amide probes in Helices 1 and 2 exceeds 35 Å. (C) Same as (B) but with the terminus extending inside the lumen so that the spin label is much closer to the affected probes. Modified from Religa et al. [39]. (For interpretation of the references to color in this figure legend, the reader is referred to the web version of this article.)

replacing the endogenous Gly4 with Cys) and the difference between amide proton relaxation rates in the presence and absence of spin label quantified, Γ_2^{NH}. Significant enhancements of relaxation rates (red circles in Fig. 6A) were obtained for amides that are localized to helices 1 and 2 (Fig. 3A), with rates of well over 100 s^{-1} for Val87 and Phe91 (helix 1). Elements of structure with elevated Γ_2^{NH} values are shown (red) in the inset to the figure. Notably, these regions are far removed from the position of the spin label (red star) in the structure of Fig. 6B which places the terminus on the outside of the proteasome (*i.e.*, above the α-annulus; recall that the conformation of these gating termini are not known from the X-ray structures). A second orientation of the terminus (Fig. 6C) is one where it extends through the annulus into the lumen of the proteasome barrel. In this conformation the distance of approach of the spin label to helices H1 and H2 can account for the attenuation pattern observed experimentally.

The results from the amide proton spin relaxation study suggest an experiment that can be used to establish the origin of the excess peaks. A spin label was placed at position 95 (Fig. 3A), where large Γ_2^{NH} values were observed, and ^{1}H–^{13}C Met spectra recorded on Y8G/D9G α_7 (identical results were obtained for WT α_7, as well). In Fig. 7A spectra recorded with (black contours) and without (red single contours) the spin label are shown. Notably all of the 'B'/'C' peaks are eliminated by the spin-label, consistent with the gating termini extending well inside the lumen of the barrel for states 'B' and 'C', as illustrated in the right most structural schematic. In contrast, very small $\Gamma_2^{CH_3}$ values of between 3 and 7 s^{-1} were obtained for the 'A' peaks, suggesting that in the 'A' conformation the gating residues are far removed from the spin-label, as would be expected for the structure indicated on the left. To confirm that this is, in fact, the case we carried out a second experiment in which the spin label was placed in a region of structure above the α-annulus (position 20), Fig. 7B. The opposite effect was now observed, whereby peaks corresponding to the 'A' state disappeared, while those derived from states 'B' and 'C' remained essentially unaffected. This is what is expected assuming that the 'A' and 'B'/'C' peaks derive from termini that are 'out' and 'in', respectively, in relation to the proteasome lumen. Note that while the 'B'/'C' correlations can be identified as 'in', the resolution of the PRE approach does not allow us to elucidate the structural differences between these two unique 'in' states.

If the 'structural' assignments described above are correct then they predict that peaks from state 'A' corresponding to gating termini that are 'out' would be affected by various modulators of proteasome activity that bind to the α_7 rings on either side of the barrel-like ($\alpha_7\beta_7\beta_7\alpha_7$) structure. One such molecule is the 11S activator [45], Fig. 8A. Placement of nitroxide spin labels on position 108 of this heptameric complex (yellow stars) is expected to eliminate peaks from Met-1/Met1/Met6 of the 'A' state since termini in this conformation would be localized to inside the 11S lumen (*i.e.*, close to the spin label), with little effect on the corresponding peaks from states 'B' and 'C' that would be within the lumen of the proteasome and hence far removed from spin label. This is exactly what was observed in binding studies involving Y8G/D9G α_7 and 11S, Fig. 8B (note that the lumen of the proteasome is below the α_7 ring) [39].

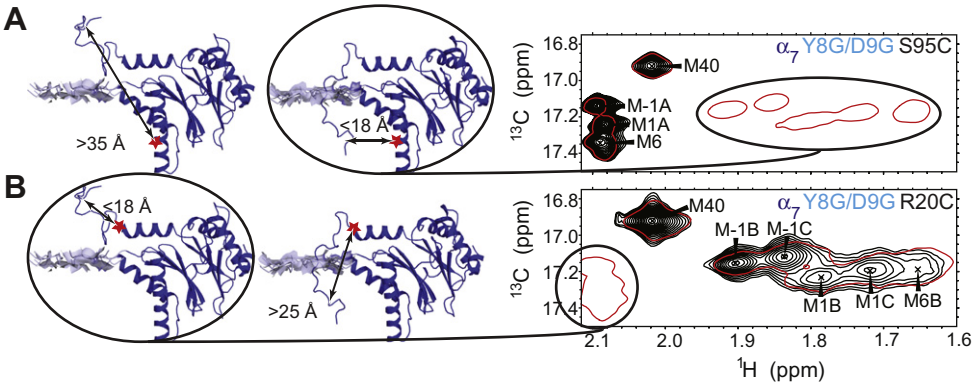

Fig. 7. (A) Superposition of ^{1}H–^{13}C Met-methyl HMQC spectra recorded of the Y8G/D9G α_7 ring showing that attachment of a spin-label at position 95 (red star, see Fig. 3A) eliminates correlations from states 'B' and 'C' for Met1, -1 and 6. These correlations must therefore be derived from the 'in' state. (B) Placement of a nitroxide at residue 20 (red star, Fig. 3A) eliminates peaks from the 'A' conformation, that must correspond therefore to the 'out' state. Shown are spectra recorded with the nitroxide in the oxidized (black) and reduced states (red; 1 contour). The R20C α_7 mutant is less stable than WT or S95C α_7, so its spectra were obtained at a lower temperature (40 °C rather than 50 °C), accounting for the increased linewidths. Modified from Religa et al. [39].

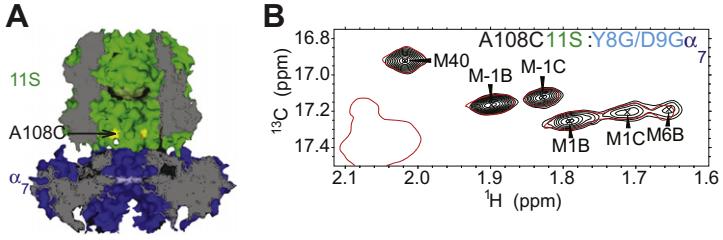

Fig. 8. (A) Space filling cross-section side-view representation of the α_7-11S complex [46], highlighting the position of the spin-label in the lumen of 11S (yellow). The spin label is placed at position 108 in each of the seven copies of the symmetric 11S heptamer. Note that termini in the 'out' position would be localized to the lumen of the 11S particle, proximal to the spin label, while those in the 'in' state would point into the lumen of the proteasome (below the α_7 ring) and hence reside distal from the nitroxide. (B) ^{1}H–^{13}C HMQC spectra of the Y8G/D9G α_7-11S complex with spin-label in the oxidized (black) and reduced (red, single contour) states. The absence of 'A' state correlations for both Met1, -1 and 6 provides very strong evidence in support of the assignments of 'A' and 'B'/'C' peaks to the 'out' and 'in' conformations, respectively. Modified from Religa et al. [39].

The PRE measurements were preformed by addition of nitroxide labels at several sites in the α-subunit, labeled in red in Fig. 3A. This provides distance constraints that can be used to calculate ensembles of gating termini structures, corresponding to 'out' and 'in'. Fig. 9A illustrates the positions of N-termini for two of the seven α-subunits comprising an α_7 ring. By residing in the lumen of the proteasome barrel, the 'in' termini decrease the size of the α-annulus that must be traversed by substrate for subsequent degradation. The more termini that are in the 'in' position, the smaller the gate area and hence access to substrate is diminished.

An important advantage of NMR over other structural techniques is that the kinetics and the thermodynamics of the process studied can often be obtained. In the case at hand, for example, it is possible to obtain the fractional populations of the 'in' and 'out' gating termini by quantifying peak volumes in fully relaxed spectra [39], Fig. 9B. Notably, in the WT α_7 ring (and in $\alpha_7\beta_7\beta_7\alpha_7$) 2 of the 7 termini are 'in'. The thermodynamics of 'out'/'in' can be manipulated by mutation at key positions as illustrated in the case of Y8G/D9G α_7, E25G α_7 and E25P α_7 where ~3, ~1 and 0 termini are displaced inwards, on average. Residues 8 and 9 are part of a reverse turn structure that stabilizes the 'out' conformation [46], while position 25 is located in helix H0 whose structural integrity is critical for the 'in' conformation. Both Gly and Pro are known to destabilize helices, with Pro having a more dramatic effect [47]. Binding of the 11S activator to the WT proteasome has been shown through biochemical studies to increase substrate degradation [46]. This observation is explained nicely by the NMR results that show a decrease in the number of 'in' termini from 2 (WT α_7) to less than 1 (WT α_7-11S), on average, thereby increasing the surface area of the α-annulus accessible to substrate, Fig. 9C. It is also known that proteasomes whose α-subunits contain the Y8G/D9G pair of mutations have no activity increase upon 11S activator binding [46]. This can also be understood from the NMR results where the distribution of 'in'/'out' termini does not change upon 11S binding, Fig. 9C (Y8G/D9G vs. GG+11S). Finally, a reasonably good correlation between rate of substrate proteolysis and α-annulus accessible surface area is shown in Fig. 9D that confirms the model of gating in the archaeal proteasome described here.

In addition to the thermodynamic data that is readily accessible from simple NMR experiments, the time-scale of termini exchange from 'in' to 'out' can also be quantified from a magnetization exchange scheme. Here spectra are recorded with ^{1}H labeling during a t_1 period that precedes a mixing element where exchange is allowed to occur, followed by ^{1}H chemical shift labeling during t_2 [39], Fig. 10A. In order to ensure that NOE-type cross-peaks are not observed in spectra a scheme is employed whereby the exchange of ^{1}H, ^{13}C longitudinal order is quantified. Cross-relaxation between proximal protons during this period creates magnetization that cannot be refocused into observable coherences. Fig. 10B shows buildup curves for the transfer of magnetization from site 'A' to 'B', 'A' to 'C' and 'B' to 'C' as monitored by Met-1. A 2D data set recorded with a mixing time T_{MIX} of 500 ms is shown in panel C, with cross-peaks arising from exchange events that interchange 'in' and 'out' conformations. From the time dependencies of diagonal- and cross-peak intensities, exchange rates can be

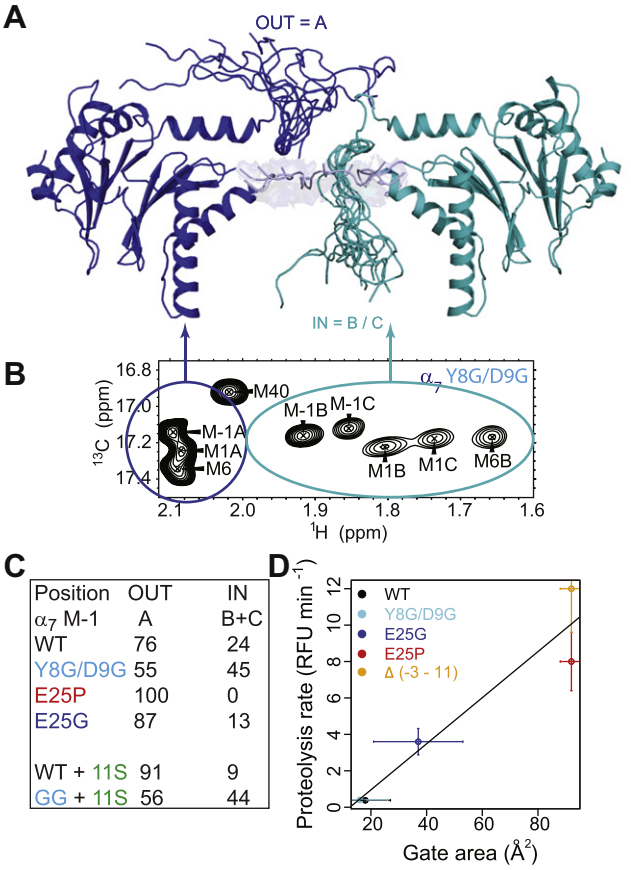

Fig. 9. (A) Ensembles of 10 structures calculated for WT α_7 showing gating residues in the 'in' (teal) and 'out' (blue) conformations for an α-subunit [39]. In WT α_7 approximately 2 of the 7 subunits are in the 'in' state. (B) Populations of 'in' and 'out' are calculated on the basis of peak volumes in spectra: 'out' = sum of all 'A' state peaks, 'in' = sum of all 'B' + 'C' state peaks. (C) Table listing the relative populations of 'out' and 'in' states for WT α_7 and a number of mutants either without or with 11S. (D) Proteolysis rates, measured in relative fluorescence units (RFU)/time, were quantified using a 9 residue peptide and plotted as a function of α-annulus accessible surface area for different $\alpha_7\beta_7\beta_7\alpha_7$ constructs. Modified from Religa et al. [39]. (For interpretation of the references to colour in this figure legend, the reader is referred to the web version of this article.)

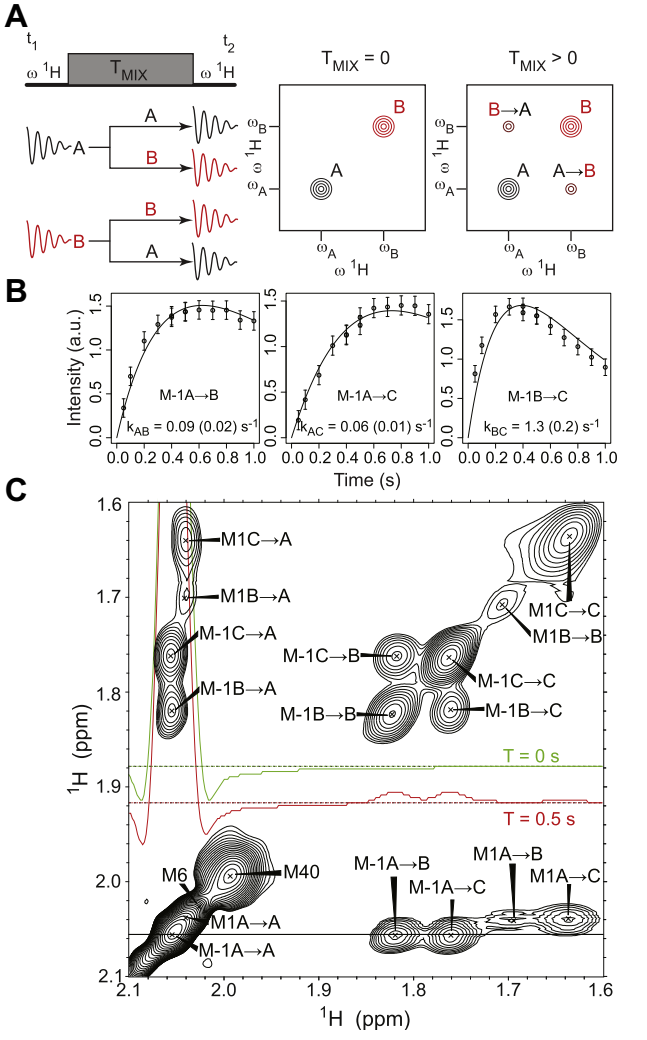

Fig. 10. (A) Schematic of the magnetization exchange experiment for measuring slow time-scale exchange events in proteins. During the mixing period, T_{MIX}, magnetization labeled by ^{13}C chemical shift in t_1 exchanges between states to produce a spectrum with both diagonal- (magnetization that has not exchanged) and cross- (exchange) peaks that can be quantified to measure the kinetics of the exchange process. (B) Buildup curves for the transfer of magnetization from sites 'A' to 'B', 'A' to 'C' and 'B' to 'C' as monitored by Met-1. (C) Exchange spectrum recorded with T_{MIX} = 0.5 s, showing both diagonal- and cross-peaks. Horizontal traces taken at the resonance position of the Met-1 peak for the 'A' state, T_{MIX} = 0 (green) and T_{MIX} = 0.5 s (red), are plotted. Modified from Sprangers et al. [62] and Religa et al. [39]. (For interpretation of the references to color in this figure legend, the reader is referred to the web version of this article.)

calculated and lifetimes of the various states determined; lifetimes on the order of 6.5 s ($(k_{AB} + k_{AC}^{-1})$) and 2 s ($\frac{1}{2}(k_{BA}^{-1} + k_{CA}^{-1})$) are obtained for the 'out' and 'in' states respectively at 45 °C [39]. Thus a picture emerges whereby gating is regulated by the stochastic interconversion of termini between a pair of conformations, 'out' and 'in', on a seconds time-scale. Such a process can clearly not be observed by techniques such as X-ray crystallography or cryo-electron microscopy that freeze specimens.

Motion of the gating residues is not restricted to the seconds time-scale; extensive dynamics have also been observed in the ps-ns time regime [39]. Before showing this data I wish to describe the underlying physics behind the method used to quantify these fast time-scale dynamics because the approach provides a nice example of how the rich network of cross-correlated spin relaxation interactions that manifest in $^{13}CH_3$ methyl groups can be exploited in yet another way. Recall that cross-correlated spin relaxation is at the essence of the methyl-TROSY effect [31], Fig. 1. To understand how it can be used in the present application consider the energy level diagram of Fig. 11A, where only the ^{1}H transitions of a methyl group are illustrated. As discussed in the context of Fig. 1, for methyls spinning rapidly and attached to macromolecules tumbling slowly, each of the ^{1}H coherences relaxes in a single exponential manner either rapidly (rate of $R_{2,H}^f$) or slowly ($R_{2,H}^s$). The non-equivalence of transverse relaxation rates can be exploited to create ^{1}H double-quantum coherence (2Q) in a methyl group even though there is no observable ^{1}H–^{1}H splitting in the ^{1}H spectrum [48,49]. The amount of 2Q coherence created, so called forbidden coherence because it is generated by the relaxation in-balance $R_{2,H}^f \neq R_{2,H}^s$ rather then by evolution of a coupling interaction [50], is related to the dynamics of the methyl group, most importantly to the square of an order parameter, S_{axis}, describing the amplitude of motion of the methyl axis [51]. Values of S_{axis}^2 can be obtained by quantifying the intensities of cross-peaks that directly report on (i) the amount of the forbidden 2Q coherence created (proportional to $\exp(-R_{2,H}^s T) - \exp(-R_{2,H}^f T)$) and (ii) the total ^{1}H magnetization (proportional to $\exp(-R_{2,H}^s T) + \exp(-R_{2,H}^f T)$) [51], Fig. 11A (right panel). This methodology has been evaluated by comparing the resulting S_{axis}^2 values obtained for the Ile, Leu, Val methyls of $\alpha_7\alpha_7$ ($^{13}CH_3$ moieties) with S_{axis}^2 quantified via ^{2}H and ^{13}C based methods using $^{13}CHD_2$ methyl

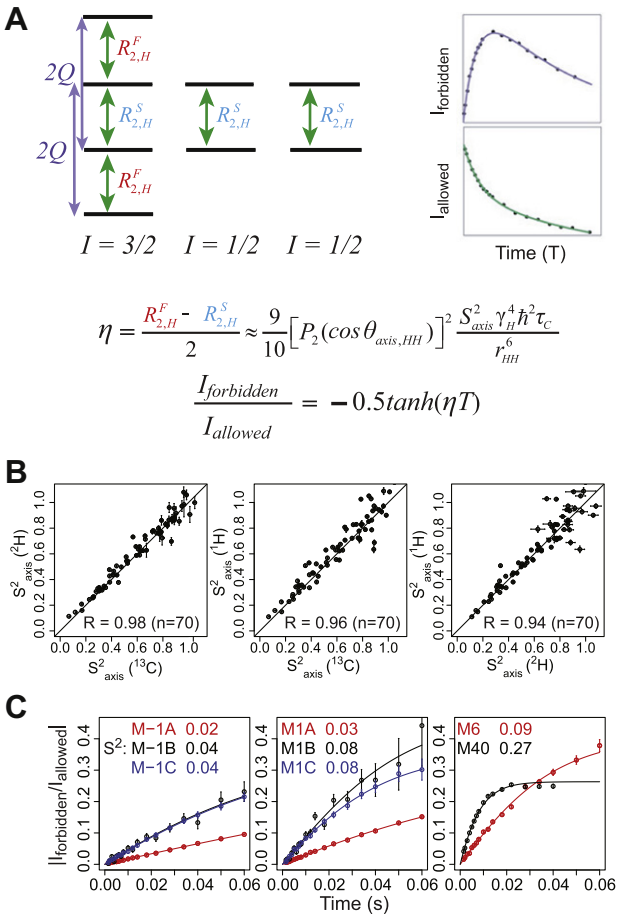

$$\eta = \frac{R^F_{2,H} - R^S_{2,H}}{2} \approx \frac{9}{10}\left[P_2(\cos\theta_{axis,HH})\right]^2 \frac{S^2_{axis}\gamma_H^4\hbar^2\tau_c}{r^6_{HH}}$$

$$\frac{I_{forbidden}}{I_{allowed}} = -0.5\tanh(\eta T)$$

Fig. 11. Energy level diagram for an X_3 spin system of a methyl group. Slow (fast) relaxing single-quantum ('allowed') ^{1}H transitions are labeled $R^S_{2,H}(R^F_{2,H})$ and are shown with green arrows. Double-quantum ('forbidden', 2Q) transitions are shown with purple arrows. Intensities of cross-peaks that are created via 2Q ($I_{forbidden}$) and single quantum ($I_{allowed}$) ^{1}H transitions are quantified to extract S^2_{axis} values [51]. (B) S^2_{axis} values derived using the methodology in (A) and obtained for the Ile, Leu, Val methyls of $\alpha_7\alpha_7$ ($^{13}CH_3$ moieties) are in good agreement with order parameters quantified via ^{2}H and ^{13}C based methods using $^{13}CHD_2$ methyl groups [38]. (C) $\frac{I_{forbidden}}{I_{allowed}}$ vs. time profiles measured for Met-1, Met1, Met6 and Met40 of WT α_7, with the values of S^2_{axis} obtained from fits of the data indicated directly above the curves. Modified from Tugarinov et al. [51] and Religa et al. [39].

groups [38], Fig. 11B, with a high level of agreement obtained [38,51].

Fig. 11C plots $\frac{I_{forbidden}}{I_{allowed}}$ vs. time profiles measured for Met-1, Met1, Met6 and Met40 of WT α_7, with the values of S^2_{axis} obtained from fits of the data indicated directly above the curves. Order parameters for Met-1, Met1 and Met6 are very low (for all states $S^2_{axis} < 0.1$) suggesting that the gating termini are not structured. By comparison $S^2_{axis} = 0.3$ for Met40 that is located in a well-structured region of the protein.

The above discussion establishes that the gating residues undergo both very slow (seconds time-scale) and very rapid (ps-ns) fluctuations. However, the absence of correlations in ^{1}H–^{15}N TROSY spectra of α_7 for the gate (Fig. 4A) [21] and the very low intensity ^{1}H–^{13}C cross-peaks for the Ile residues that were introduced into the N-termini (Fig. 4B) [39] together provides strong evidence for the presence of motion on a μs-ms time-scale as well. In order to quantify such a process we have developed a ^{1}H-based Carr–Purcell–Meiboom–Gill (CPMG) relaxation dispersion pulse scheme in which a variable number of ^{1}H 180° refocusing pulses are applied during a constant-time relaxation delay [52]. The resultant profiles plotting the transverse relaxation rate, $R_{2,\mathrm{eff}}$, vs. $\nu_{CPMG} = 1/(2\delta)$, where δ is the time between successive 180° pulses, can be fit to extract absolute values of chemical shift differences between exchanging states, $|\Delta\varpi|$, the fractional populations of such states and the kinetics of interchange [53].

The inherent spin physics of the methyl group that has been so 'accommodating' in the work that has been described to this point (*i.e.*, Methyl-TROSY, using cross-correlated ^{1}H relaxation to measure S^2_{axis}) now works against us for this application. The source of the problem can be understood by considering the energy level diagram for an H_3 methyl spin-system that highlights the fast and slowly relaxing ^{1}H coherences, Fig. 11A. Consider an application to a high molecular weight protein. The rapidly decaying transverse ^{1}H magnetization components can be ignored because they contribute little to the observed signal so that only the slowly relaxing transitions must be considered. During the constant time CPMG element a significant number of ^{1}H 180° pulses are applied and even an experienced spectroscopist cannot make them perfect. One of the effects of pulse imperfections is to interchange the proton transitions in the 3/2 manifold so that the slowly relaxing transition (corresponding to the middle transition of Fig. 11A) is converted into rapidly relaxing coherences (corresponding to the outer transitions in the diagram) that decay prior to acquisition. Since this conversion increases with the number of ^{1}H refocusing pulses until a plateau is reached, relaxation dispersion profiles are obtained where $R_{2,\mathrm{eff}}$ increases with ν_{CPMG}, the opposite of what is generally observed in the case of chemical exchange [54].

The solution to the problem is to work with a simpler spin-system that avoids the problem altogether. This can be accomplished using an AX-like spin system, well approximated by a $^{13}CHD_2$ moiety [52]. Fortunately, precursors for producing Ile, Leu, Val and Met with this labeling pattern are available commercially [55] so that preparing proteins with the requisite labeling is straightforward.

Fig. 12 plots the dispersions profiles measured using a highly deuterated $^{13}CHD_2$-Met α_7 sample for Met-1/Met1 of states 'A', 'B' and 'C' of the proteasome gate at static magnetic fields of 14.1 (black) and 18.8 T (red), 50 °C. All profiles from Met-1, Met1 and Met6 were fit simultaneously to a model of 2-site chemical exchange (solid lines). Fractional populations of exchanging states of $p_G = 94\%$ (ground, visible state) and $p_E = 6\%$ (excited, invisible state) and an interconversion rate of 1030 s^{-1} (sum of forward and reverse exchange rates) were obtained, along with $|\Delta\varpi|$ values shown in the panels in the Fig. [52]. Although the fits are reasonable, for a number of correlations it is clear that a process more complex than 2-state is likely to be operative (see insets that extend to ν_{CPMG} values of 2 kHz where the fits at high frequencies are suspect).

We have recently shown that for small protein domains (less than 100 residues) exchanging between ground (visible) and excited (invisible) states on the ms time-scale, $p_E > 0.5\%$, it is possible to measure backbone ^{1}H, ^{13}C and ^{15}N chemical shifts of the excited state via CPMG relaxation dispersion experiments not unlike the one used to generate the data of Fig. 12 [56]. These chemical shifts can, in turn, be used as restraints in structure calculations to produce atomic resolution models of the excited conformer [56,57]. The $|\Delta\varpi|$ values measured for the Met residues, Fig. 12, provide only minimal insight into the nature of the excited state, but the significant chemical shift differences relative to the ground state, in particular for conformers 'B'/'C', do suggest substantial changes in the environments of the methyl probes between ground and excited state structures.

The results of the present section establish that the archaeal proteasome gating residues are dynamic over a broad spectrum of time-scales, extending from pico-seconds to seconds. Despite the fact that the gating termini are largely unstructured they nevertheless exist in a small number of discrete states corresponding to 'in' and 'out' with respect to the lumen of the proteasome. On

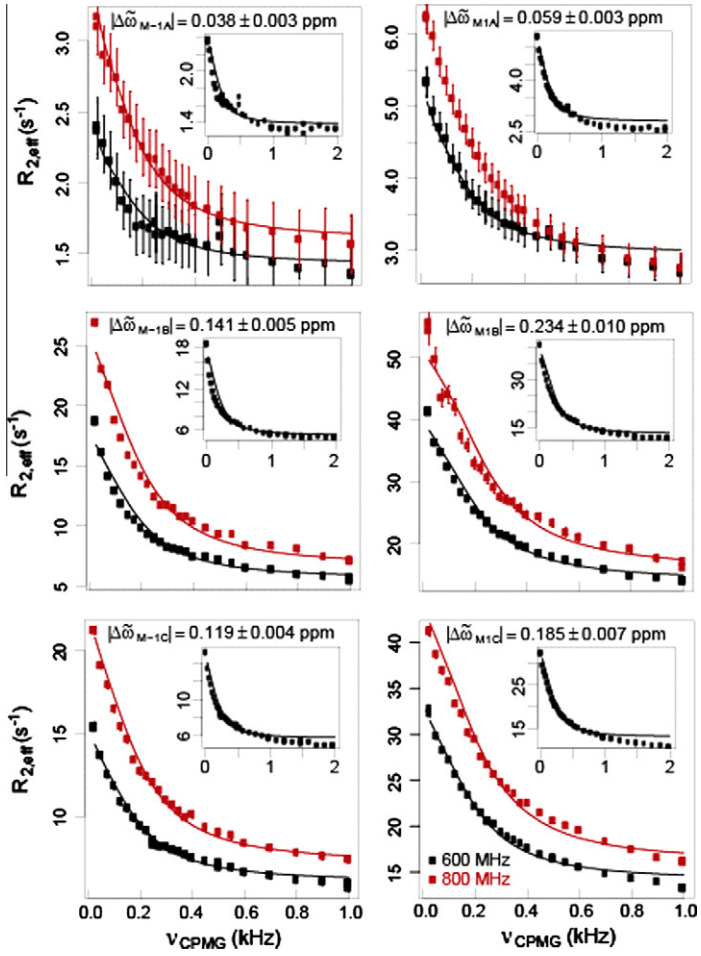

Fig. 12. ^{1}H methyl relaxation dispersion profiles for Met-1/Met1 of states 'A', 'B' and 'C' of the proteasome gate measured at static magnetic fields of 14.1 (black) and 18.8 T (red), 50 °C, fit simultaneously to a model of 2-site chemical exchange (solid lines). A highly deuterated $^{13}CHD_2$-Met α_7 sample was used. Values of $|\Delta\varpi|$ extracted from fits are shown, along with dispersion profiles to 2 kHz (inset). Reproduced from Baldwin et al. [52].

average 2 of the 7 termini in a WT α-ring extend into the barrel-like structure. The stochastic interconversion between these states provides one mechanism for controlling substrate entry and subsequent degradation [39].

3.2. Conformation and dynamics of substrate in the proteasome antechamber

Mass-spectrometry and electron microscopy studies have shown that substrates can accumulate in all three chambers of the *Thermoplasma acidophilum* 20S CP, supporting a model whereby the antechambers function as reservoirs for toxic proteins prior to degradation [58]. Although folded substrates must first be unfolded prior to entering the proteasome through the α-annuli (Fig. 3A) [42], the structural and dynamical properties of substrates once inside the proteasome antechamber has been an open question. Certainly the conformations adopted by substrates within the antechamber are critical in controlling both the rate and efficiency of protein hydrolysis. One possibility is that confinement in the antechamber would lead to the relative stabilization of the native state conformation via an entropic effect whereby the conformations accessible to the unfolded polypeptide are limited. However, refolding of substrates while they are 'stored' is undesirable as many sites would become resistant to cleavage.

Methyl-based NMR experiments of the sorts described above in the context of studies of proteasome gating are also powerful for addressing the structural and motional properties of substrate in the proteasome antechamber. In these studies stable substrate-proteasome complexes have been produced by tethering substrate molecules to the proteasome through a 15 Å heterobifunctional reagent that links the N-terminus of the substrate to a cysteine located on the surface of the α-subunit, with each antechamber populated by approximately one substrate molecule, on average [40]. Three substrate molecules have been chosen for study, including the engrailed homeodomain from *Drosophila melanogaster* (EnHD), a Fyn Src homology 3 domain from *Gallus gallus* (FynSH3) and the WW domain from human Pin1 (Pin1WW), whose properties are summarized in Fig. 13. Studies have been carried out with substrate tethered to the walls of both $\alpha_7\alpha_7$ and $\alpha_7\beta_7\beta_7\alpha_7$. The '½ proteasome' is advantageous in that the smaller molecular mass relative to the full molecule translates into higher quality data that can be quantified more accurately; however very similar results are obtained in both cases [40]. Indeed, this is not surprising given that the structures of α and β-subunits are essentially identical, with very similar amino-acid types lining the $\alpha_7\alpha_7$ and $\alpha_7\beta_7$ cavities in each case.

In a first set of experiments U-[^{2}H] Ile-[$\delta1^{13}CH_3$], Leu, Val-[$^{13}CH_3$,$^{12}CD_3$] samples of EnHD, Pin1WW and FynSH3 were produced and encapsulated within $\alpha_7\alpha_7$ or $\alpha_7\beta_7\beta_7\alpha_7$ [40]. Notably, the highly dispersed spectra characteristic of folded proteins that were obtained for the 'free' molecules were replaced by poorly dispersed maps in the case of encapsulation, with peak positions

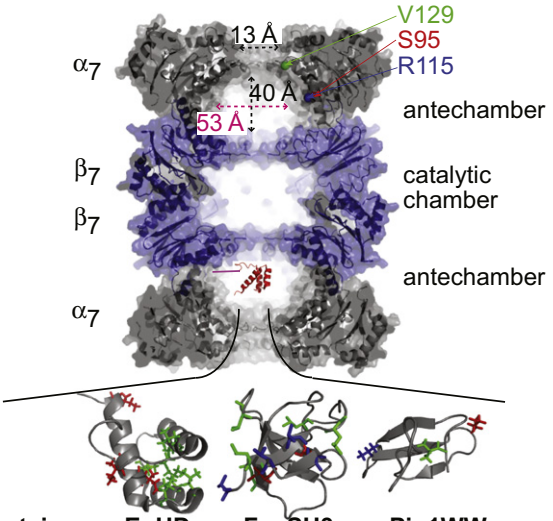

Protein	EnHD	FynSH3	Pin1WW
Fold	α-α-α	β-β-β-β-3$_{10}$-β	β-β-β
Weight (kDa)	7.7	7.6	4.4
pI	11.7	4.3	11.3
Folding	μs,3-state	ms,3-state	μs, 2-state

Fig. 13. Structure of the proteasome from *T. acidophilum* [12], highlighting the three chambers (antechamber volume = 59 nm^3; catalytic chamber volume = 84 nm^3). Substrate is encapsulated by tethering to one of three locations, Ser95, Val129, Arg115, indicated by red, green, and blue spheres respectively. The native structures of proteasome substrates EnHD, FynSH3, and Pin1WW are shown, along with the locations of Ile (red), Leu (green), and Val (blue) probes using a stick representation. Details of each fold, molecular mass, pI and folding properties are indicated. Modified from Ruschak et al. [40].

consistent with unfolded conformations. This is illustrated for EnHD in Fig. 14A. A well-resolved spectrum of the free protein is obtained at 50 °C (purple). By contrast, when EnHD is tethered to $\alpha_7\alpha_7$ all of the Leu correlations converge to only a pair of peaks (red), corresponding to the positions expected for the δ1 and δ2 methyls in the case of an unfolded protein. By means of comparison, the spectrum of temperature denatured free EnHD (80 °C) is shown in black, that looks remarkably similar to the data set obtained of the encapsulated molecule at 50 °C. Similar results were obtained for the other substrates as well, Fig. 14B. It is worth noting that unfolding upon encapsulation is not the result of linking substrate to a particular position in the cavity since very similar spectra were generated with tethering at a variety of locations, Fig. 14A inset. Moreover, when substrate was linked to the outside of $\alpha_7\alpha_7$ the protein remained folded. Clearly, there is something unique about the inside of the cavity that destabilizes substrates.

In order to explore the nature of the interactions between substrate and cavity $S^2_{axis}\tau_C$ values have been measured for methyl groups of Pin1WW linked to $\alpha_7\alpha_7$ (50 °C), where τ_C is the correlation time of the assumed isotropically tumbling substrate [40]. Values of $S^2_{axis}\tau_C$ range between 30 and 50 ns, Fig. 15A (blue); in comparison $S^2_{axis}\tau_C \sim 1$ ns is obtained for residues of free Pin1WW at 50 °C (red), while $S^2_{axis}\tau_C$ values of ~70 ns are quantified, on average, for Ile, Leu and Val methyl groups of $\alpha_7\alpha_7$ (gray). The similarity of the dynamics parameters for methyls attached to encapsulated substrate and to $\alpha_7\alpha_7$ suggests that the substrate interacts strongly with the cavity walls. In fact, assuming that the encapsulated WW domain tumbles with the same correlation time as the ½ proteasome (125 ns) values of S^2_{axis} between 0.27 and 0.41 are obtained, consistent with the degree of ordering expected for methyl groups of an unfolded polypeptide chain [59].

Since the spin relaxation experiments establish that there are interactions between substrate and cavity we were interesting in determining whether the contacts were specific. A series of PRE experiments were recorded where spin label was attached to EnHD that was subsequently tethered to U-[^{2}H] Ile-[$\delta1^{13}CH_3$], Leu, Val-[$^{13}CH_3$,$^{12}CD_3$]-$\alpha_7\alpha_7$. Intensities of methyl correlations in ^{1}H–^{13}C HMQC spectra were recorded in the presence (I_{ox}) and absence (I_{red}) of spin label. In Fig. 15B the ratio I_{ox}/I_{red} (Y-axis) is plotted for each methyl group of $\alpha_7\alpha_7$, ordered according to proximity to the cavity surface (X-axis) for a nitroxide at position 24 of the substrate. An essentially identical pattern of intensity attenuation is obtained when the spin label is positioned at residue 58 (R^2 = 0.98), Fig. 15C. Thus, different residues of EnHD do not have unique, position-dependent interactions with the cavity surface suggesting that the substrate is best described in terms of an ensemble of dynamic, interconverting unfolded conformations.

Taken together the experimental results summarized in this section establish that the proteasome antechamber maintains

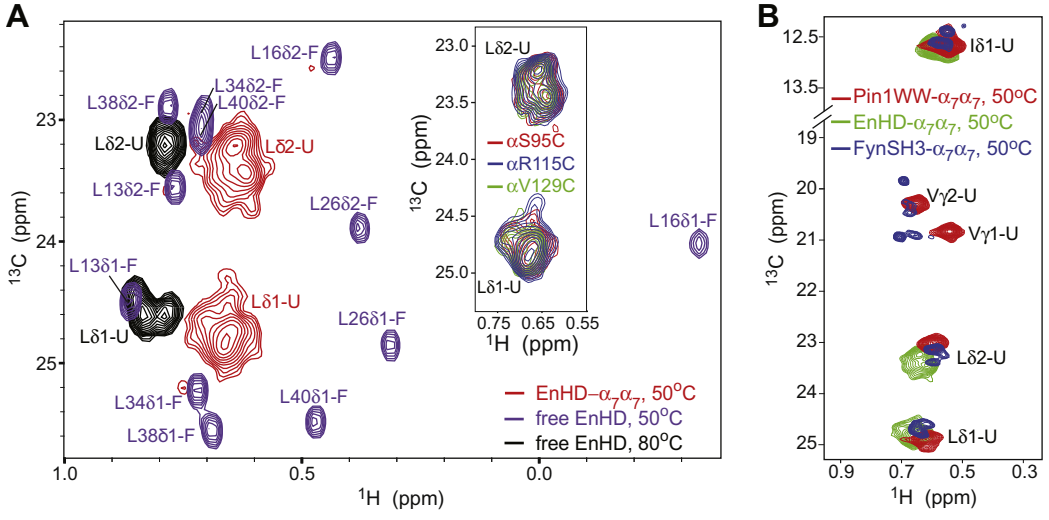

Fig. 14. (A) Spectrum of the Leu region of EnHD tethered to position 95 of the α-subunit in $\alpha_7\alpha_7$ (red; on average there is one substrate per cavity) and free in solution (purple), 50 °C. For reference the spectrum of the temperature denatured state of free EnHD is shown at 80 °C (black). ^{1}H–^{13}C HMQC spectra of EnHD tethered to residues 95 (red), 115 (blue), and 129 (green) of α in $\alpha_7\alpha_7$, 50 °C are shown in the inset. (B) Superimposed spectra of EnHD (green), Pin1WW (red), and FynSH3 (blue) encapsulated at position 95 of $\alpha_7\alpha_7$, 50 °C, showing that all three substrate are unfolded. Modified from Ruschak et al. [40].

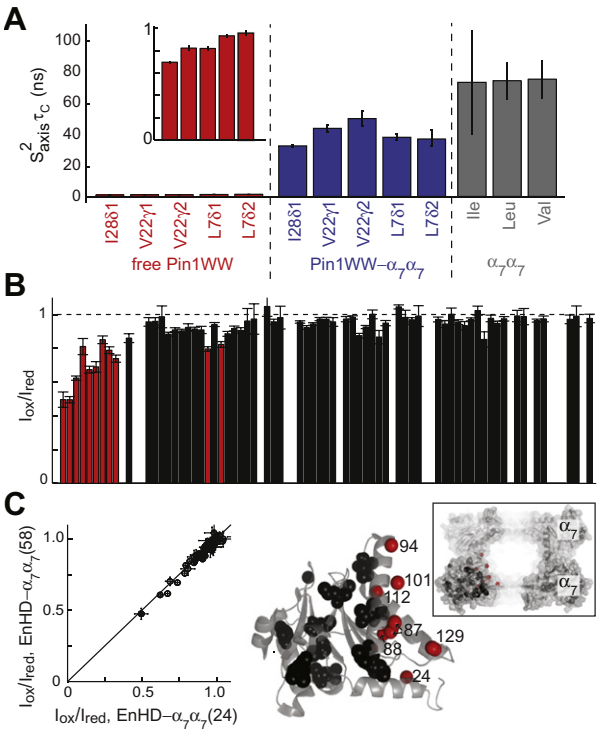

Fig. 15. (A) $S^2_{axis}\tau_C$ values for Ile, Leu, Val probes in free Pin1WW (red), in Pin1WW encapsulated into $\alpha_7\alpha_7$ (blue) and in $\alpha_7\alpha_7$ (gray, average values for the 65% of methyl groups which are intermediate in the distribution for each residue type are indicated, along with standard deviation as error bars). (B) I_{ox}/I_{red} values for ILV methyl groups in $\alpha_7\alpha_7$ resulting from attachment of a TEMPO nitroxide spin label to residue 24 of encapsulated EnHD. Ratio of intensities measured for all methyl groups arranged in order of their proximity to the inside surface (left to right, groups are located increasingly farther from the surface; red bars correspond to >10% peak attenuation). (C) Values of I_{ox}/I_{red} in (B) are compared with the corresponding ratios obtained for EnHD conjugated with TEMPO at residue 58. In both cases the substrate is tethered to Ser95 of the α-subunit. Positions of α-subunit methyl groups whose peaks show >10% (red), or <10% (black) intensity changes upon addition of nitroxide-labeled EnHD in $\alpha_7\alpha_7$ are highlighted on a single α particle whose orientation in the context of $\alpha_7\alpha_7$ is indicated. Modified from Ruschak et al. [40].

substrate in an unfolded conformation so as to 'prime' it for proteolysis [40]. In this sense the antechamber must be considered as an 'active' chamber that interacts directly with substrate and destabilizes it. On the basis of the diverse set of substrates considered here (see Fig. 13) it appears that these interactions are, at least to a significant extent, independent of substrate secondary structure, topology, folding properties and surface charge.

4. Concluding remarks

In this perspective I have presented several examples showing that solution NMR spectroscopy can be used to provide insight into how a molecular machine – the proteasome – functions. The work builds upon the high resolution, static X-ray structures of the proteasome that have been produced in the past 15 years. I have specifically highlighted questions that cannot be addressed properly by any technique that produces static pictures for which specimens in the solid state are required. The goal of solution NMR studies of large supra-molecular complexes should not be to replicate what is available from other methods at higher resolution and in a much more straightforward manner. Rather, the most useful role of NMR in this case is to serve as a complement to other structural techniques by deciphering the role of molecular dynamics in function. It seems likely that the importance of NMR in this capacity will only increase as the number of high resolution X-ray structures continues to grow.

Acknowledgments

Work described in this perspective is supported by a grant from the Canadian Institutes of Health Research. I am very much indebted to Drs. Remco Sprangers, Tomasz Religa and Amy Ruschak for their tremendous efforts in the proteasome studies that my laboratory has conducted over the past 5 years and for their help, along with that of Dr. Algirdas Velyvis and Professor Vitali Tugarinov, in preparing figures for this manuscript. Dr. J. Forman-Kay is thanked for a critical reading of the manuscript.

References

[1] A.C. Gavin, P. Aloy, P. Grandi, R. Krause, M. Boesche, M. Marzioch, C. Rau, L.J. Jensen, S. Bastuck, B. Dumpelfeld, A. Edelmann, M.A. Heurtier, V. Hoffman, C. Hoefert, K. Klein, M. Hudak, A.M. Michon, M. Schelder, M. Schirle, M. Remor, T. Rudi, S. Hooper, A. Bauer, T. Bouwmeester, G. Casari, G. Drewes, G. Neubauer, J.M. Rick, B. Kuster, P. Bork, R.B. Russell, G. Superti-Furga, Proteome survey reveals modularity of the yeast cell machinery, Nature 440 (2006) 631–636.
[2] M. Karplus, J. Kuriyan, Molecular dynamics and protein function, Proc. Natl Acad. Sci. USA 102 (2005) 6679–6685.
[3] J. Deisenhofer, O. Epp, K. Miki, R. Huber, H. Michel, X-ray structure analysis of a membrane protein complex. Electron density map at 3 A resolution and a model of the chromophores of the photosynthetic reaction center from Rhodopseudomonas viridis, J. Mol. Biol. 180 (1984) 385–398.
[4] M. Roth, A. Lewitbentley, H. Michel, J. Deisenhofer, R. Huber, D. Oesterhelt, Detergent structure in crystals of a bacterial photosynthetic reaction center, Nature 340 (1989) 659–662.
[5] J.P. Abrahams, A.G. Leslie, R. Lutter, J.E. Walker, Structure at 2.8 A resolution of F1-ATPase from bovine heart mitochondria, Nature 370 (1994) 621–628.
[6] P. Cramer, D.A. Bushnell, J. Fu, A.L. Gnatt, B. Maier-Davis, N.E. Thompson, R.R. Burgess, A.M. Edwards, P.R. David, R.D. Kornberg, Architecture of RNA polymerase II and implications for the transcription mechanism, Science 288 (2000) 640–649.
[7] P. Cramer, D.A. Bushnell, R.D. Kornberg, Structural basis of transcription: RNA polymerase II at 2.8 angstrom resolution, Science 292 (2001) 1863–1876.
[8] B.T. Wimberly, D.E. Brodersen, W.M. Clemons Jr., R.J. Morgan-Warren, A.P. Carter, C. Vonrhein, T. Hartsch, V. Ramakrishnan, Structure of the 30S ribosomal subunit, Nature 407 (2000) 327–339.
[9] N. Ban, P. Nissen, J. Hansen, P.B. Moore, T.A. Steitz, The complete atomic structure of the large ribosomal subunit at 2.4 A resolution, Science 289 (2000) 905–920.
[10] F. Schluenzen, A. Tocilj, R. Zarivach, J. Harms, M. Gluehmann, D. Janell, A. Bashan, H. Bartels, I. Agmon, F. Franceschi, A. Yonath, Structure of functionally activated small ribosomal subunit at 3.3 angstroms resolution, Cell 102 (2000) 615–623.
[11] K. Braig, Z. Otwinowski, R. Hegde, D.C. Boisvert, A. Joachimiak, A.L. Horwich, P.B. Sigler, The crystal structure of the bacterial chaperonin GroEL at 2.8 A, Nature 371 (1994) 578–586.
[12] J. Lowe, D. Stock, B. Jap, P. Zwickl, W. Baumeister, R. Huber, Crystal structure of the 20S proteasome from the archaeon *T. acidophilum* at 3.4 Å resolution, Science 268 (1995) 533–539.
[13] F. Bonneau, J. Basquin, J. Ebert, E. Lorentzen, E. Conti, The yeast exosome functions as a macromolecular cage to channel RNA substrates for degradation, Cell 139 (2009) 547–559.
[14] J.M. Grimes, J.N. Burroughs, P. Gouet, J.M. Diprose, R. Malby, S. Zientara, P.P. Mertens, D.I. Stuart, The atomic structure of the bluetongue virus core, Nature 395 (1998) 470–478.
[15] F. Castellani, B. van Rossum, A. Diehl, M. Schubert, K. Rehbein, H. Oschkinat, Structure of a protein determined by solid-state magic-angle-spinning NMR spectroscopy, Nature 420 (2002) 98–102.
[16] C. Wasmer, A. Lange, H. Van Melckebeke, A.B. Siemer, R. Riek, B.H. Meier, Amyloid fibrils of the HET-s(218–289) prion form a beta solenoid with a triangular hydrophobic core, Science 319 (2008) 1523–1526.
[17] A. Bax, Multidimensional nuclear magnetic resonance methods for protein studies, Curr. Opin. Struct. Biol. 4 (1994) 738–744.
[18] G.M. Clore, A.M. Gronenborn, Structures of larger proteins in solution: three- and four-dimensional heteronuclear NMR spectroscopy, Science 252 (1991) 1390–1399.
[19] A. Velyvis, Y.R. Yang, H.K. Schachman, L.E. Kay, A solution NMR study showing that active site ligands and nucleotides directly purturb the allosteric equilibrium in aspartate transcarbamolyase, Proc. Natl. Acad. Sci. USA 104 (2007) 8815–8820.
[20] A. Velyvis, H.K. Schachman, L.E. Kay, Application of methyl-TROSY NMR to test allosteric models describing effects of nucleotide binding to aspartate transcarbamoylase, J. Mol. Biol. 387 (2009) 540–547.

[21] R. Sprangers, X. Li, X. Mao, J.L. Rubinstein, A.D. Schimmer, L.E. Kay, TROSY-based NMR evidence for a novel class of 20S proteasome inhibitors, Biochemistry 47 (2008) 6727–6734.
[22] R. Sprangers, A. Gribun, P.M. Hwang, W.A. Houry, L.E. Kay, Quantitative NMR spectroscopy of supramolecular complexes: dynamic side pores in ClpP are important for product release, Proc. Natl. Acad. Sci. USA 102 (2005) 16678–16683.
[23] I. Gelis, A.M. Bonvin, D. Keramisanou, M. Koukaki, G. Gouridis, S. Karamanou, A. Economou, C.G. Kalodimos, Structural basis for signal-sequence recognition by the translocase motor SecA as determined by NMR, Cell 131 (2007) 756–769.
[24] N.K. Goto, K.H. Gardner, G.A. Mueller, R.C. Willis, L.E. Kay, A robust and cost-effective method for the production of Val, Leu, Ile (δ1) methyl-protonated 15N-, 13C-, 2H-labeled proteins, J. Biomol. NMR 13 (1999) 369–374.
[25] V. Tugarinov, L.E. Kay, An isotope labeling strategy for methyl TROSY spectroscopy, J. Biomol. NMR 28 (2004) 165–172.
[26] I. Ayala, R. Sounier, N. Use, P. Gans, J. Boisbouvier, An efficient protocol for the complete incorporation of methyl-protonated alanine in perdeuterated protein, J. Biomol. NMR 43 (2009) 111–119.
[27] R.L. Isaacson, P.J. Simpson, M. Liu, E. Cota, X. Zhang, P. Freemont, S. Matthews, A new labeling method for methyl transverse relaxation-optimized spectroscopy NMR spectra of alanine residues, J. Am. Chem. Soc. 129 (2007) 15428–15429.
[28] M. Fischer, K. Kloiber, J. Hausler, K. Ledolter, R. Konrat, W. Schmid, Synthesis of a 13C-methyl-group-labeled methionine precursor as a useful tool for simplifying protein structural analysis by NMR spectroscopy, ChemBioChem 8 (2007) 610–612.
[29] A.M. Ruschak, A. Velyvis, L.E. Kay, A simple strategy for (1)(3)C, (1)H labeling at the Ile-gamma2 methyl position in highly deuterated proteins, J. Biomol. NMR 48 129–135.
[30] P. Gans, O. Hamelin, R. Sounier, I. Ayala, M.A. Dura, C. Amero, M. Noirclerc-Savoye, B. Franzetti, M.J. Plevin, J. Boisbouvier, Stereospecific isotopic labeling of methyl groups for NMR spectroscopic studies of high molecular weight proteins, Angew. Chem. Int. Ed. 49 (2010) 1958–1962.
[31] V. Tugarinov, P. Hwang, J. Ollerenshaw, L.E. Kay, Cross-correlated relaxation enhanced 1H–13C NMR spectroscopy of methyl groups in very high molecular weight proteins and protein complexes, J. Am. Chem. Soc. 125 (2003) 10420–10428.
[32] L.E. Kay, D.A. Torchia, The effects of dipolar cross-correlation on ^{13}C methyl-carbon T_1, T_2 and NOE measurements in macromolecules, J. Magn. Reson. 95 (1991) 536–547.
[33] A. Bax, R.H. Griffey, B.L. Hawkings, Correlation of proton and nitrogen-15 chemical shifts by multiple quantum NMR, J. Magn. Reson. 55 (1983) 301–315.
[34] L. Mueller, Sensitivity enhanced detection of weak nuclei using heteronuclear multiple quantum coherence, J. Am. Chem. Soc. 101 (1979) 4481–4484.
[35] K. Pervushin, R. Riek, G. Wider, K. Wüthrich, Attenuated T_2 relaxation by mutual cancellation of dipole-dipole coupling and chemical shift anisotropy indicates an avenue to NMR structures of very large biological macromolecules in solution, Proc. Natl Acad. Sci. USA 94 (1997) 12366–12371.
[36] D.J. Hamel, F.W. Dahlquist, The contact interface of a 120 kD CheA-CheW complex by methyl TROSY interaction spectroscopy, J. Am. Chem. Soc. 127 (2005) 9676–9677.
[37] C. Amero, P. Schanda, M.A. Dura, I. Ayala, D. Marion, B. Franzetti, B. Brutscher, J. Boisbouvier, Fast two-dimensional NMR spectroscopy of high molecular weight protein assemblies, J. Am. Chem. Soc. 131 (2009) 3448–3449.
[38] R. Sprangers, L.E. Kay, Quantitative dynamics and binding studies of the 20S proteasome by NMR, Nature 445 (2007) 618–622.
[39] T.L. Religa, R. Sprangers, L.E. Kay, Dynamic regulation of archaeal proteasome gate opening as studied by TROSY NMR, Science 328 (2010) 98–102.
[40] A.M. Ruschak, T.L. Religa, S. Breuer, S. Witt, L.E. Kay, The proteasome antechamber maintains substrates in an unfolded state, Nature 467 (2010) 868–871.
[41] A.L. Goldberg, Protein degradation and protection against misfolded or damaged proteins, Nature 426 (2003) 895–899.
[42] W. Baumeister, J. Walz, F. Zuhl, E. Seemuller, The proteasome: paradigm of a self-compartmentalizing protease, Cell 92 (1998) 367–380.
[43] A.L. Goldberg, Functions of the proteasome: from protein degradation and immune surveillance to cancer therapy, Biochem. Soc. Trans. 35 (2007) 12–17.
[44] A. Mittermaier, L.E. Kay, J.D. Forman-Kay, Analysis of deuterium relaxation-derived methyl axis order parameters and correlation with local structure, J. Biomol. NMR 13 (1999) 181–185.
[45] F.G. Whitby, E.I. Masters, L. Kramer, J.R. Knowlton, Y. Yao, C.C. Wang, C.P. Hill, Structural basis for the activation of 20S proteasomes by 11S regulators, Nature 408 (2000) 115–120.
[46] A. Forster, E.I. Masters, F.G. Whitby, H. Robinson, C.P. Hill, The 1.9 A structure of a proteasome-11S activator complex and implications for proteasome-PAN/PA700 interactions, Mol. Cell 18 (2005) 589–599.
[47] A. Fersht, Structure and Mechanism in Protein Science, W.H. Freeman and Company, New York, 1999.
[48] L.E. Kay, J.H. Prestegard, Methyl group dynamics from relaxation of double quantum filtered NMR signals-application to deoxycholate, J. Am. Chem. Soc. 109 (1987) 3829–3835.
[49] N. Muller, G. Bodenhausen, R.R. Ernst, Relaxation-induced violations of coherence transfer selection rules in nuclear magnetic resonance, J. Magn. Reson. 75 (1987) 297–334.
[50] R.R. Ernst, G. Bodenhausen, A. Wokaun, Principles of Nuclear Magnetic Resonance in One and Two Dimensions, Oxford University Press, Oxford, 1987.
[51] V. Tugarinov, R. Sprangers, L.E. Kay, Probing side-chain dynamics in the proteasome by relaxation violated coherence transfer NMR spectroscopy, J. Am. Chem. Soc. 129 (2007) 1743–1750.
[52] A.J. Baldwin, T.L. Religa, D.F. Hansen, G. Bouvignies, L.E. Kay, (13)CHD(2) methyl group probes of millisecond time scale exchange in proteins by (1)H relaxation dispersion: an application to proteasome gating residue dynamics, J. Am. Chem. Soc. 132 (2010) 10992–10995.
[53] A.G. Palmer, C.D. Kroenke, J.P. Loria, NMR methods for quantifying microsecond-to-millisecond motions in biological macromolecules, Methods Enzymol. 339 (2001) 204–238.
[54] D.M. Korzhnev, A.K. Mittermaier, L.E. Kay, Cross-correlated spin relaxation effects in methyl 1H CPMG-based relaxation dispersion experiments: complications and a simple solution, J. Biomol. NMR 31 (2005) 337–342.
[55] V. Tugarinov, L.E. Kay, Methyl groups as probes of structure and dynamics in NMR studies of high-molecular-weight proteins, ChemBioChem 6 (2005) 1567–1577.
[56] P. Vallurupalli, D.F. Hansen, L.E. Kay, Structures of invisible, excited protein states by relaxation dispersion NMR spectroscopy, Proc. Natl. Acad. Sci. USA 105 (2008) 11766–11771.
[57] D.M. Korzhnev, T.L. Religa, W. Banachewicz, A.R. Fersht, L.E. Kay, A transient and low-populated protein-folding intermediate at atomic resolution, Science 329 (2010) 1312–1316.
[58] M. Sharon, S. Witt, K. Felderer, B. Rockel, W. Baumeister, C.V. Robinson, 20S proteasomes have the potential to keep substrates in store for continual degradation, J. Biol. Chem. 281 (2006) 9569–9575.
[59] W.Y. Choy, D. Shortle, L.E. Kay, Side chain dynamics in unfolded protein states: an NMR based ^2H spin relaxation study of Δ131Δ, J. Am. Chem. Soc. 125 (2003) 1748–1758.
[60] K. Stieglitz, B. Stec, D.P. Baker, E.R. Kantrowitz, Monitoring the transition from the T to the R state in *E. coli* aspartate transcarbamoylase by X-ray crystallography: crystal structures of the E50A mutant enzyme in four distinct allosteric states, J. Mol. Biol. 341 (2004) 853–868.
[61] J. Wang, J.A. Harting, J.M. Flanagan, The structure of ClpP at 2.3 Å resolution suggests a model for ATP-dependent proteolysis, Cell 91 (1997) 447–456.
[62] R. Sprangers, A. Velyvis, L.E. Kay, Solution NMR of supramolecular complexes: providing new insights into function, Nat. Methods 4 (2007) 697–703.